Raman forward scattering and self-modulation of laser pulses in tapered plasma channels

J. R. Peñano, B. Hafizi,* P. Sprangle, R. F. Hubbard, and A. Ting
Plasma Physics Division, Beam Physics Branch, Naval Research Laboratory, Washington, D.C. 20375
(Received 26 March 2002; published 17 September 2002)

The propagation of intense laser pulses with durations longer than the plasma period through tapered plasma channels is investigated theoretically and numerically. General propagation equations are presented and reduced partial differential equations that separately describe the forward Raman (FR) and self-modulation (SM) instabilities in a nonuniform plasma are derived. Local dispersion relations for FR and SM instabilities are used to analyze the detuning process arising from a longitudinal density gradient. Full-scale numerical fluid simulations indicate parameters that favorably excite either the FR or SM instability. The suppression of the FR instability and the enhancement of the SM instability in a tapered channel in which the density increases longitudinally is demonstrated. For a pulse undergoing a self-modulation instability, calculations show that the phase velocity of the wakefield in an untapered channel can be significantly slower than the pulse group velocity. Simulations indicate that this wake slippage can be forestalled through the use of a tapered channel.

DOI: 10.1103/PhysRevE.66.036402 PACS number(s): 52.38.−r, 41.75.Jv, 52.38.Hb

I. INTRODUCTION

Intense laser pulses propagating through plasma channels can be utilized in a broad range of applications such as x-ray generation [1], advanced laser fusion schemes [2,3], and plasma-based accelerators [4]. It is possible that the next generation of laser wake field accelerator (LWFA) experiments will use tapered plasma channels to guide short, intense laser pulses over long distances (many Rayleigh lengths) to achieve GeV electron energies. By tapered, it is meant that the plasma density and channel radius can vary along the propagation path of the laser pulse. Allowing the density to increase in the direction of propagation is advantageous for accelerator applications because the phase velocity of the wake field behind the laser pulse is increased [5,6]. The density variation can be optimally configured to create luminal regions in the wake field where electron dephasing (the process by which energetic electrons outrun the accelerating and focusing regions of the wake) can be forestalled for extended distances [7,8].

Numerical simulations of short pulses in untapered channels have demonstrated stable propagation over many tens of Rayleigh lengths and have shown the possibility of accelerating electrons to ~ 1 GeV energies [9,10]. In addition, simulations using tapered channels indicate that ~ 4 GeV energies are possible [8]. While these results are promising, the laser and channel requirements for an experimental demonstration of a GeV accelerator are difficult to realize at present. For example, the short-pulse GeV accelerator proposed in Ref. [8] requires a plasma channel of length 0.5–1 m with an on-axis density on the order of $10^{17}\,\mathrm{cm}^{-3}$. While segmented capillary discharges [11] can be used to taper the density and, in principle, can be used to create arbitrarily long plasma channels, it is difficult to create densities below $10^{18}\,\mathrm{cm}^{-3}$ using this technique. Operating at densities of $\sim 10^{18}\,\mathrm{cm}^{-3}$ places most lasers in the standard or long-pulse regimes, i.e., $c\tau_L \geqslant \lambda_p$, where τ_L is the pulse duration and λ_p is the plasma wavelength. Hence, it is useful to study channel propagation in the long-pulse regime in order to better understand present-day experiments and to determine viable experiments that can be done in the near future.

It is often observed in experiments that when the laser power, P, exceeds the critical power for self-focusing, P_p, the laser pulse becomes self-guided [12–14] and energetic electrons are produced [15–18]. However, the self-guiding process can only be maintained for several (~ 5) Rayleigh lengths. Guiding over much longer distances using preformed plasma channels has been experimentally demonstrated [19–22] and simulations [9,10,23] of channel-guided pulses exhibit strong pulse modulation and wake field generation. However, rapid phase slippage in untapered channels is also observed [8,23], which could severely limit the energy gain. Using a tapered channel may make it possible to partially overcome this dephasing limitation and make the channel-guided self-modulated LWFA a viable candidate for near-term accelerator experiments.

Pulses with durations $c\tau_L > \lambda_p$ propagating in plasmas are subject to Raman instabilities [24–28]. Although the forward Raman (FR) instability has a growth rate that is smaller than that of the backward Raman instability, it is perhaps more disruptive since it can remain within the pulse for extended distances and grow to a large amplitude. The backward Raman instability can act as a seed for the FR instability [29,30]. The FR instability is fundamentally a one-dimensional (1D) process that arises from the longitudinal bunching of energy within the laser pulse. The bunching is associated with the near-resonant scattering of photons into Stokes and anti-Stokes sidebands which are shifted from the laser carrier frequency by the plasma frequency. As the instability progresses, the laser envelope becomes modulated at the plasma frequency and wakefields are generated. In plasma channels, the FR instability is affected by the radial variation of the plasma frequency and proceeds differently than in a homogeneous plasma [34].

The self-modulation (SM) instability [31–33] also produces envelope modulations at the plasma frequency and

*Mailing address: Icarus Research, Inc., P.O. Box 30780, Bethesda, MD 20824-0780.

generates wake fields. It differs from the FR instability in that it is not a 1D process and arises from focusing due to the transverse variations in the wake field [33]. The SM instability is enhanced by relativistic self-focusing.

For long pulses, the FR and SM instabilities can interact for parameters relevant to plasma-based accelerator applications. The coupling of FR and SM instabilities in untapered plasma channels was analyzed by Esarey *et al.* [40]. Both instabilities, however, are also affected by longitudinal variations in the plasma density such as in the case of a tapered channel. In a tapered channel, the resonance condition for a particular Stokes sideband is satisfied only in a localized spatial region. As the laser pulse propagates out of the interaction region, the FR instability for that spectral band is detuned and growth is limited. This detuning process was analyzed by Rosenbluth [35] and considered heuristically by McKinstrie and Bingham [26]. However, the growth rate of the FR instability increases with the plasma density. Hence, in a tapered channel in which the density increases in the direction of propagation, the detuning effect may be compensated by the increasing local growth rate. For a channel in which the density decreases along the propagation path, both the detuning effect and the decrease in plasma density act to suppress the FR instability. The longitudinal density variation also causes the critical power for relativistic self-focusing to vary along the propagation path. The variation of the focusing power can affect the SM instability.

This paper examines theoretically and numerically the effects of a tapered plasma channel on the FR and SM instabilities and on the wake fields generated by these instabilities. The basic equations governing laser pulse propagation in a tapered channel are presented in Sec. II. In Sec. III, the general propagation equations are used to derive reduced equations that separately describe the FR and SM instabilities in a plasma with a longitudinal density variation. Section IV contains a heuristic analysis of detuning caused by a longitudinal density gradient. Section V presents results of full-scale numerical simulations of propagation in tapered channels. Conclusions are presented in Sec. VI.

II. GENERAL FORMULATION

In this section, the basic equations describing the propagation of a laser pulse in a tapered plasma channel are presented. The laser pulse, plasma channel, and the coordinate axes are illustrated schematically in Fig. 1. It is assumed that the laser electric field is linearly polarized and can be written in terms of a slowly varying, dimensionless complex envelope, $A(\mathbf{r},t)$, and a rapidly varying phase $\psi(z,t) = \int_0^z k_0(z')\,dz' - \omega_0 t$, i.e.,

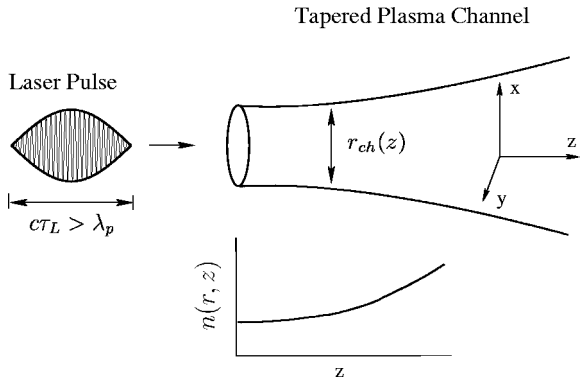

FIG. 1. Schematic illustration of a laser pulse and a tapered plasma channel.

$$\mathbf{E}(\mathbf{r},t) = \frac{1}{2}(mc\omega_0/e)A(\mathbf{r},t)\exp[i\psi(z,t)]\hat{\mathbf{y}} + \text{c.c.}, \quad (1)$$

where e and m are the fundamental units of charge and electron mass, respectively, c is the speed of light in vacuum, ω_0 is the angular laser frequency, and c.c. denotes the complex conjugate. The plasma channel is characterized by a spatially varying density of the form

$$N(r,z) = n(z)[1 + r^2/r_{ch}^2(z)], \quad (2)$$

where $r_{ch}(z)$ and $n(z)$ denote the longitudinally varying channel radius and on-axis plasma density, respectively. The parabolic radial variation of the density allows for the guiding of a laser beam with a transverse Gaussian profile, i.e., $A \propto \exp(-r^2/r_0^2)$ when the channel radius is [8]

$$r_{ch}(z) = \frac{k_p(z) r_0^2}{2\sqrt{1 - P/P_p(z)}}, \quad (3)$$

where P is the laser power, $P_p(z) = 2(m^2c^5/e^2) \times [\omega_0/\omega_p(z)]^2$ is the critical power for nonlinear self-focusing in a plasma [36,37], $k_p(z) = \omega_p(z)/c = 2\pi/\lambda_p(z)$, and $\omega_p(z) = \sqrt{4\pi e^2 n(z)/m}$ is the plasma frequency on axis.

The equations governing the evolution of the laser envelope are then given by [8]

$$\left[\nabla_\perp^2 + \frac{4}{r_0^2} - k_p^2(z)\frac{r^2}{r_{ch}^2(z)} + 2ik_0(z)\left(1 + \frac{i}{k_0(z)v_g(z)}\frac{\partial}{\partial\tau}\right)\frac{\partial}{\partial z} + i\frac{\partial k_0(z)}{\partial z}\left(1 + \frac{i}{k_0(z)v_g(z)}\frac{\partial}{\partial\tau}\right) + \left(\frac{1}{v_g^2(z)} - \frac{1}{c^2}\right)\frac{\partial^2}{\partial\tau^2} + k_p^2(z) \times \left(\frac{e}{m\omega_p^2(z)}\nabla\cdot\mathbf{E}_w + \frac{|A|^2}{4}\right)\right]A(\mathbf{r},z,\tau) = 0 \quad (4)$$

and

$$\left[\frac{\partial^2}{\partial\tau^2}+\Omega_p^2(r,z)\right]\mathbf{E}_w=-\frac{mc^2}{4e}\Omega_p^2(r,z)\nabla|A|^2, \qquad (5)$$

where $r=\sqrt{x^2+y^2}$ is the radial coordinate, r_0 is the initial laser spot size, $\Omega_p(r,z)=\sqrt{4\pi e^2N(r,z)/m}$, and $\mathbf{E}_w$ is the ponderomotively excited wake electric field which produces a density perturbation δn given by

$$\frac{\delta n}{n(z)}=-\frac{e}{m\omega_p^2(z)}\nabla\cdot\mathbf{E}_w. \qquad (6)$$

The divergence operator is given by $\nabla=\nabla_\perp+\hat{z}[(\partial/\partial z)-v_g^{-1}(\partial/\partial\tau)]$. The coordinate system (x,y,z,τ) is associated with a reference frame moving at instantaneous velocity $v_g(z)$; the independent variable z denotes propagation distance and $\tau=t-\int_0^z dz'/v_g(z')$ measures time relative to the arrival of the laser pulse at location z. The quantity $|A|=(e/mc\omega_0)\langle 2\mathbf{E}\cdot\mathbf{E}\rangle^{1/2}$, where $\langle\rangle$ denotes a time average, is the magnitude of the electron oscillation momentum normalized to mc.

In writing Eqs. (4) and (5), it has been assumed that the weakly relativistic limit, i.e., $|A|^2<1$, applies. Also, in deriving Eq. (4) a small term proportional to $\partial^2A/\partial z^2$ has been neglected. Neglecting this term is equivalent to neglecting backscattered waves. Hence, the backward Raman instability is omitted. Otherwise, Eq. (4) is correct to order $|A|^3$. In deriving Eq. (5) the term $c^2\nabla\times\nabla\times\mathbf{E}_w$, which appears on the left side [38,39], has been neglected. Neglecting this term is valid when $1/k_p\ll r_0\ll r_{ch}$.

The wave number k_0 is given by

$$k_0(z)=c^{-1}\sqrt{\omega_0^2-4c^2/r_0^2-\omega_p^2(z)}, \qquad (7)$$

and the transformation velocity v_g has been set equal to the linear group velocity of the laser, i.e.,

$$v_g(z)=c^2k_0(z)/\omega_0. \qquad (8)$$

Equations (4) and (5) describe laser pulse propagation subject to the effects of group velocity dispersion, relativistic self-focusing, self-phase modulation, and optical guiding by a preformed tapered plasma channel. Plasma group velocity dispersion is included through the term in Eq. (4) proportional to $\partial^2A/\partial\tau^2$ [40,41]. Relativistic self-focusing [42,43] and self-phase modulation are introduced though the term proportional to $|A|^3$. Optical guiding by the plasma channel is obtained by balancing the first three terms on the right hand side of Eq. (4). Additionally, the term proportional to the mixed derivative $\partial^2A/\partial\tau\partial z$ can lead to the longitudinal bunching of energy; neglecting this term is equivalent to making the paraxial approximation [40]. The radial variation of the channel density in Eq. (5) causes curvature of the plasma wave wave fronts and a damping of the wakefield in the longitudinal direction [44].

Equations (4) and (5) can describe both the FR and SM instabilities. The forward Raman instability arises fundamentally from a longitudinal bunching of energy which gives rise to a modulation of the laser envelope on the scale of the plasma wavelength. In Eq. (4), the FR instability in the four-wave resonant regime arises through the combined effects of the wakefield and mixed derivative terms. The self-modulation instability also modulates the laser envelope at the plasma frequency, however, this is accomplished through transverse focusing provided by the radial variation of the plasma wakefield [33]. The SM instability is retained in Eq. (4) through a combination of the density perturbation term and the transverse Laplacian operator. The mixed derivative term can be neglected for SM, i.e., the paraxial approximation can be made. Additionally, the relativistic term can be neglected for a fundamental description of SM, although as we will show, relativistic focusing can enhance its growth.

III. REDUCED EQUATIONS

Reduced equations that separately describe the FR and SM instabilities for propagation in a plasma with a longitudinally varying density, $N(z)$, can be derived from the general propagation equations. We begin with Eqs. (4), (5), and (6), but neglect the plasma channel, group velocity dispersion, and the spot size correction terms. It is also assumed that the longitudinal variation of the carrier wave number, k_0, and group velocity, v_g, can be neglected. These approximations are valid when the pulse dimensions and channel radius are much larger than $1/k_p$, $\omega_p\ll\omega_0$, and the growth rates of instabilities are much larger than c/Z_R, where $Z_R=k_0(0)r_0^2/2$ is the Rayleigh length. With these approximations, Eq. (4) can be written approximately as

$$\frac{\partial A}{\partial z}=\frac{i}{2k_0}\left(1-\frac{i}{k_0v_g}\frac{\partial}{\partial\tau}\right)(\nabla_\perp^2-k_p^2\Phi)A, \qquad (9)$$

where $\Phi=\delta n/n-|A|^2/4$, and it has been assumed that $|\partial A/\partial\tau|\ll k_0v_g$.

When the growth rates of the instabilities are much smaller than the plasma frequency, the operator ∇, when acting on fields, can be approximated by $\nabla\approx\nabla_\perp-(\hat{z}/v_g)\partial/\partial\tau$, which is equivalent to making the quasistatic approximation [45]. This allows Eqs. (5) and (6) to be combined into a single scalar equation for Φ given by

$$\left[\frac{\partial^2}{\partial\tau^2}+\omega_p^2(z)\right]\Phi=\frac{1}{4}[c^2\nabla_\perp-\omega_p^2(z)]|A|^2, \qquad (10)$$

where the term $(1/4)(c^2/v_g^2-1)(\partial^2|A|^2/\partial\tau^2)$ has been neglected from the right side under the assumption that $v_g\approx c$.

To proceed with the analysis of Eqs. (9) and (10), the fields are represented as

$$A=a_0+a_+(z,\tau)e^{i\theta}+a_-(z,\tau)e^{-i\theta}, \qquad (11)$$

and

$$\Phi=\phi_0+[\phi(z,\tau)e^{i\theta}+\text{c.c.}], \qquad (12)$$

where $\phi_0 = -a_0^2/4$ and $\theta(\mathbf{r}_\perp, z, \tau) = \mathbf{k}_\perp \cdot \mathbf{r}_\perp - \omega_p(z)\tau$ is taken to be a real function of $\mathbf{r}_\perp = x\hat{x} + y\hat{y}$, z, and τ. The complex envelopes $a_\pm$ and ϕ contain the growth of the instabilities and are assumed to vary slowly in τ compared with θ.

Substituting Eqs. (11) and (12) into Eqs. (9) and (10) results in

$$\frac{\partial}{\partial z}(a_+ e^{-i\omega_p\tau}) = -\frac{ie^{-i\omega_p\tau}}{2k_0}\left[1 - \frac{i}{k_0 v_g}\left(\frac{\partial}{\partial\tau} - i\omega_p\right)\right] \times [k_p^2 a_0\phi + k_\perp^2 a_+], \tag{13}$$

$$\frac{\partial}{\partial z}(a_-^* e^{-i\omega_p\tau}) = \frac{ie^{-i\omega_p\tau}}{2k_0}\left[1 + \frac{i}{k_0 v_g}\left(\frac{\partial}{\partial\tau} - i\omega_p\right)\right] \times [k_p^2 a_0\phi + k_\perp^2 a_-^*], \tag{14}$$

$$\frac{\partial\phi}{\partial\tau} = \frac{-ia_0}{8\omega_p}(c^2k_\perp^2 + \omega_p^2)(a_+ + a_-^*). \tag{15}$$

In deriving Eqs. (13) and (14), terms proportional to $\phi_0 a_\pm$, which are small compared with ϕa_0, have been neglected on the right side.

Setting $k_\perp = 0$, allows Eqs. (13), (14), and (15) to be combined into a single equation for ϕ which describes Raman forward scattering in an inhomogeneous plasma, i.e.,

$$\left[\frac{\partial^2}{\partial z\partial\tau} - \frac{\gamma_{FR}^2(z)}{v_g}\right]\phi = \left[\frac{\partial}{\partial z}\ln\left(\frac{e^{-i\omega_p\tau}}{\omega_p}\right)\right]\frac{\partial\phi}{\partial\tau}, \tag{16}$$

where the right side contains only terms that are proportional to the gradient of the plasma density. The quantity $\gamma_{FR}(z) = a_0\omega_p^2(z)/\sqrt{8}\omega_0$ is the standard expression for the local peak temporal growth rate of FR in a rarefied plasma [25,26] in which the Stokes and anti-Stokes waves are driven resonantly, i.e., four-wave growth. For cases where ω_p/ω_0 cannot be neglected compared with unity, the anti-Stokes wave is driven nonresonantly and can be neglected. In this limit, Eqs. (14) and (15) can be combined into an equation for ϕ identical in form to Eq. (16), but with $\gamma_{FR}(z) = a_0\{[1 + (\omega_p/\omega_0)](\omega_p/\omega_0)\}^{1/2}\omega_p/4$, which is the standard expression for the peak temporal growth rate in the three-wave regime [26].

In the limit of a homogeneous plasma, i.e., $\omega_p'(z) = 0$, Eq. (16) reduces to

$$\left[\frac{\partial^2}{\partial z\partial\tau} - \frac{\gamma_{FR}^2}{v_g}\right]\phi = 0, \tag{17}$$

which is identical in form to the quasistatic limit of Eq. (10) of Ref. [28]. Equation (17) has the asymptotic solution $\phi \sim \exp[2\gamma_{FR}\sqrt{z\tau/v_g}]$.

For a weakly inhomogeneous plasma, the right side of Eq. (16) can be neglected leading to an approximate solution given by

$$\phi(z,\tau) \sim \exp\left[2\left(\frac{\tau}{v_g}\int^z \gamma_{FR}^2(z')\,dz'\right)^{1/2}\right]. \tag{18}$$

Equation (18) is valid in the regime $\tau \gg 1/\omega_p$, $z \ll L$, and for $\sqrt{z\tau} \ll 2L\gamma_{FR}/\omega_p\sqrt{v_g}$, where $L = [(\partial\omega_p^2/\partial z)/\omega_p]^{-1}$ is the density gradient scale length.

An equation describing the self-modulation instability in an inhomogeneous plasma is obtained from Eqs. (13), (14), and (15) by making the paraxial approximation, i.e., neglecting the $\partial/\partial\tau$ operator on the right side of Eq. (9). To derive a single equation describing the SM instability, it is convenient to let $a_\pm(z,\tau) = \overline{a}_\pm(z,\tau)\exp(\pm i\Delta z)$, $\phi(z,\tau) = \overline{\phi}(z,\tau)\exp(i\Delta z)$ and define $\hat{a}_\pm(z,\tau) = \overline{a}_\pm\exp[\mp i\omega_p(z)\tau]$ and $\hat{\phi}(z,\tau) = \overline{\phi}\exp[-i\omega_p(z)\tau]$. With the paraxial approximation, choosing $\Delta = -k_\perp^2/2k_0$ allows Eqs. (13) and (14) to be written more simply as

$$\frac{\partial\overline{a}_+}{\partial z} = -i\frac{k_p^2 a_0}{2k_0}\overline{\phi}, \tag{19}$$

$$\left(\frac{\partial}{\partial z} + 2i\Delta\right)\overline{a}_-^* = i\frac{k_p^2 a_0}{2k_0}\overline{\phi}. \tag{20}$$

Equations (19) and (20) can be combined with Eq. (15) into a single equation for $\hat{a}_-^*$ given by

$$c^2\frac{\partial}{\partial z}\left\{\frac{e^{-i\omega_p\tau}}{\omega_p^3}\frac{\partial}{\partial\tau}\left[e^{i\omega_p\tau}\left(\frac{\partial}{\partial z} + 2i\Delta\right)\hat{a}_-^*\right]\right\} = ig^2\hat{a}_-^*, \tag{21}$$

where $g = a_0k_\perp/4k_0$. Equation (21) describes the self-modulation instability in a plasma with a longitudinal density variation.

In the uniform plasma limit Eq. (21) reduces to

$$\frac{1}{c}\frac{\partial^3\overline{a}_-^*}{\partial\tau\partial z^2} = ig^2k_p^3\overline{a}_-^*, \tag{22}$$

where the term $2i\Delta\hat{a}_-^*$ is assumed to be small in comparison with $\partial\hat{a}_-^*/\partial z$ and has been neglected. This assumption is valid when $k_\perp/k_p \ll (a_0^2k_0/k_p)^{1/4}$. Equation (22), which is identical in form to Eq. (52) of Ref. [33], has an asymptotic solution of the form [31,33]

$$\overline{a}_-^* \sim \exp\left[3\left(\frac{\sqrt{3}}{2} + \frac{i}{2}\right)\left(\frac{1}{4}g^2k_p^3z^2c\tau\right)^{1/3}\right]. \tag{23}$$

IV. HEURISTIC THEORY

In this section, we present a heuristic analysis of parametric instabilities in an inhomogeneous plasma similar to that presented by McKinstrie and Bingham in Ref. [26]. This will prove useful for interpreting results from the full scale numerical simulations presented in Sec. V.

In a spatially uniform and underdense plasma, with the assumption that $v_g \approx c$, the complex envelopes can be expressed as monochromatic perturbations of the form $\sim\exp[i(\delta k - \delta\omega/c)z - i\delta\omega\tau]$, where $\delta k \equiv k - k_p$, and k is taken to be real and $\delta\omega$ complex. In the lab frame (z,t), this is equivalent to writing, for example, $\Phi = \phi_0 + \{\phi\exp[ikz$

$-(\omega_p+\delta\omega)t]+$c.c.$\}$. In a uniform plasma, a resonant wave number ($k=k_p$) will grow until pump depletion, electron trapping, or other nonlinear mechanisms saturate the instability. In an inhomogeneous plasma, the growth of certain spectral bands can be limited by detuning. For a plasma with $k_p(z)$, detuning is defined as the process by which a perturbation with wave number $k=k_p(z_0)$ is stabilized as the laser pulse propagates a sufficient distance away from z_0 to make $k_p(z)$ change by an amount greater than the spectral width of the Raman line. Hence, unstable bands in k space translate into spatially localized regions of interaction where particular wave numbers are amplified. The width and location of the interaction regions and the maximum amount of growth expected for a given spectral band can be estimated from a calculation of the local growth rate, which will be a function of z and k. We consider the case where the scale length of inhomogeneity is much larger than the local e folding length of the instability. Hence, at every location z, it is assumed that the local growth rate is approximately equal to the homogeneous plasma growth rate. The homogeneous plasma growth rates for FR and SM due to monochromatic perturbations can be calculated from Eqs. (17) and (22).

For the following analysis, we consider a specific case where the plasma density increases linearly with z, i.e.,

$$\omega_p(z)=\omega_{p0}(1+z/L)^{1/2}, \tag{24}$$

where ω_{p0} and L are positive constants.

A. Forward Raman instability

Assuming $\phi\sim\exp[i(\delta k-\delta\omega/c)z-i\delta\omega\tau]$, in Eq. (17) results in

$$\delta\omega=\frac{1}{2}[c\,\delta k+i\sqrt{4\gamma_{FR}^2-c^2\delta k^2}]. \tag{25}$$

Maximum exponential growth with $\delta\omega=i\gamma_{FR}$ is obtained when $\delta k=0$. Writing $\delta k(z)=k-k_p(z)$, the normalized local growth rate for the four-wave interaction is given by

$$\hat{\gamma}=\frac{1}{2}\{4\hat{\gamma}_0^2(1+\hat{z})^2-[(1+\hat{z})^{1/2}-\hat{k}]^2\}^{1/2}, \tag{26}$$

for $4\hat{\gamma}_0^2(1+\hat{z})^2>[(1+\hat{z})^{1/2}-\hat{k}]^2$ and zero otherwise. The normalized quantities are $\hat{\gamma}=\mathrm{Im}(\delta\omega)/\omega_{p0}$, $\hat{k}=kc/\omega_{p0}$, $\hat{z}=z/L$, and $\hat{\gamma}_0=a_0\omega_{p0}/\sqrt{8}\omega_0$, i.e., the four-wave Raman growth rate at $z=0$ normalized to ω_{p0}.

Figure 2 shows the dependence of the growth rate given by Eq. (26) on $\hat{z}$ for several values of $\hat{k}$. Because of the spatial variation of the plasma density, each wave number $\hat{k}$ is unstable only in limited spatial region of width, $\Delta z\approx 8L\hat{k}^3\hat{\gamma}_0$. The peak growth rate, for wave number $\hat{k}$ is given by $\gamma_{max}\approx\omega_{p0}\hat{k}^2\hat{\gamma}_0$, which occurs at location $z_0\approx L(\hat{k}^2-1)$. In general, the number of e foldings experienced by a given spectral component $\hat{k}$ after propagating a distance $\hat{z}$ is given by $\Gamma(\hat{z},\hat{k})=(L\omega_{p0}/c)\int_0^z\hat{\gamma}(\hat{z}',\hat{k})\,d\hat{z}'$. Carrying out the integration over the unstable region

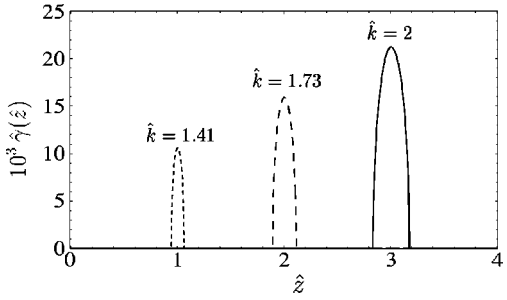

FIG. 2. Scaled local growth rate $\hat{\gamma}$ calculated from Eq. (26) vs $\hat{z}$ for $a_0=0.15$, $\omega_{p0}/\omega_0=0.1$, and $\hat{k}=1.41$, 1.73, and 2.

$-\Delta z/2<z-z_0<\Delta z/2$, the maximum number of e foldings of a given spectral component is approximately given by

$$\Gamma(\infty,\hat{k})\approx 2\pi(L\omega_{p0}/c)\hat{k}^5\hat{\gamma}_0^2. \tag{27}$$

In writing Eq. (27), the assumption $\Delta z/L\ll\hat{k}^2$ has been made. Equation (27) is consistent with the result derived by Rosenbluth [35] using a more rigorous WKB analysis.

For comparison with simulations it is useful to apply this type of analysis to a situation in which a laser pulse propagates through a plasma with a given density scale length L and a finite length L_p. Figure 3 shows plots of $\Gamma(L_p/L,\hat{k})$, i.e., the number of e foldings at $z=L_p$, for $L_p=3L$ and several values of the pump amplitude a_0. The maximum number of e foldings is seen to increase with $\hat{k}$ until $\hat{k}\approx 2$, and then decrease sharply thereafter. The increase in Γ for $\hat{k}<2$ is due to the $\hat{k}^5$ scaling mentioned previously. The cutoff at $\hat{k}\approx 2$ is due to the finite plasma length, i.e., for these parameters, $\hat{k}>2$ implies $z_0>L_p$. In practice, the number of e foldings may be less than Γ due to saturation. If we choose an arbitrary saturation level of $\Gamma=5$, then we can draw the following conclusions from Fig. 3. First, for pulses with sufficiently small a_0, the forward Raman instability can be suppressed by detuning, i.e., growth does not reach saturation levels, as indicated by the $a_0=0.08$ curve in Fig. 3. Second, for sufficiently large a_0, the wave number that reaches saturation first should decrease as a_0 increases. This can be seen by comparing the $a_0=0.15$ and $a_0=0.25$ curves in Fig. 3. Note that for the curves labeled $a_0=0.15$ and $a_0=0.25$, a

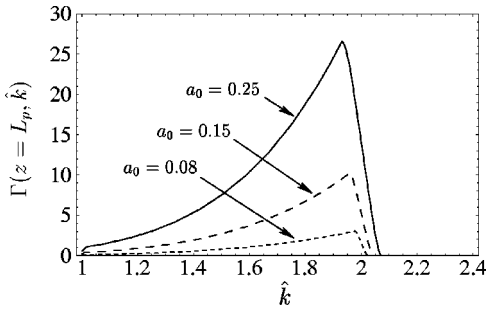

FIG. 3. Number of e foldings at $z=L_p$ vs scaled wave number $\hat{k}$ for $a_0=0.08$, 0.15, and 0.25. Plasma parameters are $\omega_p(0)/\omega_0=0.1$, $L\omega_p(0)/c=2\times 10^3$, and scaled plasma length $L_p/L=3$.

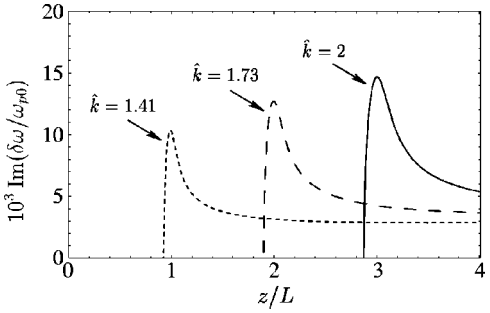

FIG. 4. Scaled SM growth rate vs z/L for $\hat{k}=1.41$, 1.73, and 2 obtained by solving Eq. (28) with $a_0=0.5$, $k_\perp c/\omega_{p0}=0.2$, $L\omega_{p0}/c=4\times10^3$, and $\omega_0/\omega_{p0}=30$.

given Γ is associated with two different values of $\hat{k}$. Because each $\hat{k}$ is unstable in a distinct spatial region as shown in Fig. 2, the smaller $\hat{k}$ should saturate the instability first.

B. Self-modulation instability

Assuming $\bar{a}_-^* \sim \exp[i(\delta k-\delta\omega/c)z-i\delta\omega\tau]$, in Eq. (22) results in a dispersion relation which is cubic in $\delta\omega$, i.e.,

$$\delta\bar{\omega}(\delta\bar{\omega}-\delta\bar{k})^2=g^2, \tag{28}$$

where $\delta\bar{\omega}=\delta\omega/\omega_p$, $\delta\bar{k}=\delta k/k_p$.

Unstable wave numbers are those for which the discriminant of the cubic is positive. This condition can be written as

$$k-k_p<\left(\frac{27}{4}g^2\right)^{1/3}k_p, \tag{29}$$

which shows that there is a broad range of unstable wave numbers. The peak growth rate occurs at $k=k_p$, i.e.,

$$\delta\omega|_{\delta k=0}=\left(-\frac{1}{2}+i\frac{\sqrt{3}}{2}\right)g^{2/3}\omega_p. \tag{30}$$

We consider a linearly varying density as given by Eq. (24) and solve Eq. (28) numerically, letting $k_p\rightarrow k_p(z)$ to obtain the local growth rate as a function of $\hat{z}$ and $\hat{k}$. Figure 4 plots the scaled growth rate versus z for several values of scaled wave number $\hat{k}=kc/\omega_{p0}$. The parameters used for the plot, i.e., $a_0=0.5$, $k_\perp c/\omega_{p0}=0.2$, $L\omega_{p0}/c=4\times10^3$, and $\omega_0/\omega_{p0}=30$ correspond closely with parameters used in full-scale simulations presented in the following section. As seen from Fig. 4, the peak growth rate for a given k occurs when $k=k_p$ or equivalently, at $z_0=L[(kc/\omega_{p0})^2-1]$. The region of instability, however, is not highly localized about z_0. Hence, for propagation into an increasing plasma density, wave numbers that initially satisfy the resonance condition $k=k_p$ at some z_0, will remain unstable for $z>z_0$, unlike the case for the FR instability in which an unstable wave number becomes stable after propagating a distance of $\approx 8L\hat{k}^3\hat{\gamma}_0$.

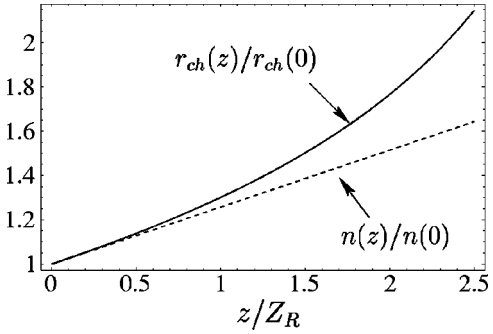

FIG. 5. Dependence of scaled channel radius and on-axis plasma density on z. Plasma density is given by $n(z)=n(0)(1+z/L)$ where $L=4\,Z_R$. Channel radius is given by Eq. (3).

V. NUMERICAL SIMULATIONS

This section presents numerical simulations of propagation in tapered plasma channels. The simulations render the laser pulse on a 3D Cartesian (x,y,τ) grid and use Eqs. (4) and (5) to advance the laser pulse in z. The approximation $\nabla\approx\nabla_\perp-(\hat{z}/v_g)\partial/\partial\tau$ is made in order to facilitate the numerical integration. This approximation requires that the scale length of the longitudinal density variation is long compared with the e folding length of any observed instability.

The seeding of the FR and SM instabilities as well as their subsequent growth can be influenced by the initial pulse shape. In all of the simulations, the initial laser envelope $(z=0)$, is taken to have the form $A=a_0\exp(-r^2/r_0^2)\cos(\pi\tau/\tau_L)$ for $-\tau_L/2<\tau<\tau_L/2$ and zero otherwise. The plasma channel is characterized by Eqs. (2) and (3) with the longitudinal variation of the on-axis density given by Eq. (24). The channel radius is chosen to vary this way so that, in the absence of instability, the pulse and channel are matched. When setting the channel radius, the power P appearing in Eq. (3) is chosen to be $P_0/\sqrt{2}$, where P_0 is the initial peak laser pulse power. Figure 5 shows an example of the characteristic variation of $n(z)$ and $r_{ch}(z)$ for the channels used in the simulations. Propagation in tapered and untapered channels will be compared. The simulations are categorized according to whether the FR or SM instability is the dominant process.

A. Forward Raman instability

According to the heuristic analysis, there are parameter regimes of the forward Raman instability where certain spectral components can grow to saturation, and regimes where the growth of all spectral components of a given laser pulse can be suppressed by the longitudinal density gradient of a tapered channel (see Fig. 3). The simulations will address these two regimes.

The first set of simulations are in the parameter regime where the instability is expected to grow to saturation. As a first case, we consider a laser pulse with $a_0=0.15$, $\lambda=1\,\mu$m, $r_0=12.6\,\mu$m, and $\tau_L=0.48$ ps propagating through a tapered channel with $n(0)=1.24\times10^{19}\,\mathrm{cm}^{-3}$ and $L=6.7\,Z_R$. For these parameters $P_0/P_p(0)=0.05$. The parameters are chosen to correspond to the curve labeled a_0

$=0.15$ in Fig. 3. Hence, the analysis of Sec. IV predicts that the $k \approx 1.8\omega_p(0)/c$ mode will e fold ≈ 7 times within a region of width $\Delta z \approx 1.7 Z_R$ in the neighborhood of $z = 15 Z_R$.

Figure 6(a) shows the resulting on-axis Fourier transform of the laser pulse at $25 Z_R$ in an untapered channel with on-axis density $n(0) = 1.24 \times 10^{19}\,\mathrm{cm}^{-3}$. Multiple Stokes and anti-Stokes lines are observed with a dominant Stokes signal at $\omega - \omega_0 = \omega_p$. Figure 6(b) shows the on-axis spectrum at $z = 17 Z_R$ after propagating through a tapered channel. The peak of the dominant Stokes sideband has grown ≈ 10 e foldings from its initial amplitude and is shifted from the pump by $\omega \approx -1.7\omega_p(0)$. At $z = 17 Z_R$ there is no appreciable signal at $\omega \approx \omega_p(0)$ due to the detuning of these spectral components by the spatial variation of the plasma density. For both the tapered and untapered cases, the Stokes sideband is approximately three times larger in amplitude than the anti-Stokes sideband indicating that the simulations are marginally in the four-wave Raman regime.

The evolution of the Stokes sideband for the simulation of Fig. 6 is illustrated in Fig. 7. Figure 7(a) compares the growth of the dominant Stokes line for a tapered and untapered channel. In the untapered channel, the Stokes line grows immediately after the start of the simulation. The Stokes wave grows exponentially for $z > 7 Z_R$ with a growth

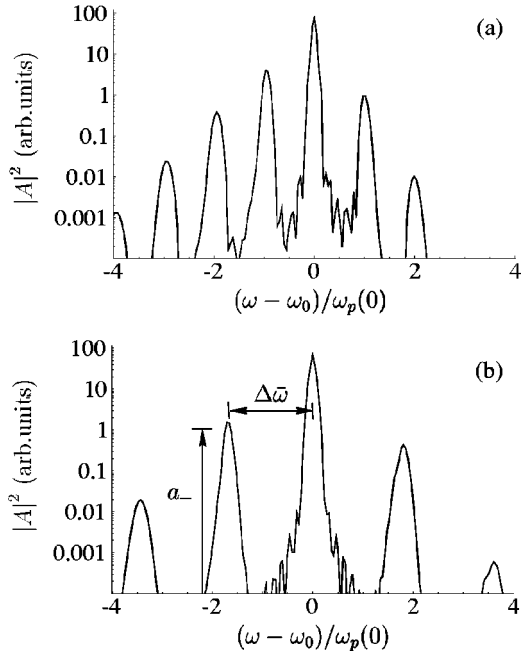

FIG. 6. On-axis frequency spectrum of a laser pulse at (a) $z = 25 Z_R$ in an untapered channel and at (b) $z = 17 Z_R$ in a tapered channel. Propagation distances are chosen such that Stokes lines undergo a similar number of e foldings between the two cases. The quantity $\Delta\bar{\omega}$ in panel (b) denotes the frequency separation between the pump and the Stokes sideband normalized to $\omega_p(0)$. The quantity a_- denotes the amplitude of the first Stokes sideband. The initial laser pulse has $a_0 = 0.15$, $\lambda = 1\ \mu$m, $r_0 = 12.6\ \mu$m, and $\tau_L = 0.48$ ps. The on-axis plasma density at $z = 0$ is $n(0) = 1.24 \times 10^{19}\,\mathrm{cm}^{-3}$. At $z = 0$, $P_0/P_p(0) = 0.05$. For the tapered channel, $L = 6.7 Z_R$.

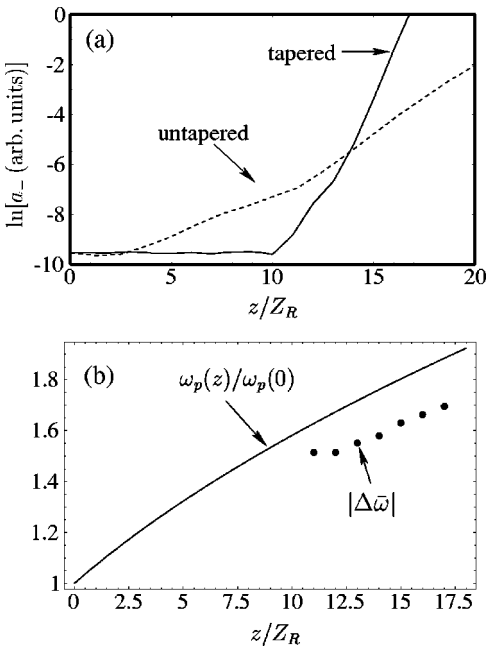

FIG. 7. (a) Amplitude of the Stokes sidebands vs z for the tapered and untapered plasma channels from the simulations of Fig. 6. (b) Normalized frequency shift of the Stokes sideband, $\Delta\bar{\omega}$, vs z for the tapered channel simulation of Fig. 6(b). The solid curve in panel (b) denotes the normalized plasma frequency.

rate that is roughly 3.5 times smaller than the standard four-wave Raman growth rate. In the tapered channel, the growth of the Stokes wave is delayed. No discernable Stokes line is observed until $z > 10 Z_R$. The suppression of the Stokes line for $z < 10 Z_R$ is consistent with the detuning process discussed in Sec. IV. Figure 7(b) shows the evolution of the normalized frequency shift of the Stokes line for the tapered channel. The Stokes frequency shift increases with the local plasma frequency but is smaller than the plasma frequency by a constant amount $\approx 0.2\omega_p(0)$. The Stokes shift at a given z is equal to the plasma frequency at approximately $z - 3Z_R$.

Figure 8 shows the laser power and on-axis intensity profiles associated with the spectra shown in Fig. 6. The fact that the power and intensity profiles exhibit a similar degree of modulation indicates that the modulations arise mainly from a longitudinal bunching of energy within the laser pulse, which is characteristic of the FR instability. The modulations are also seen to damp faster towards the back of the pulse for the tapered channel case.

Assuming that the FR instability is saturated, i.e., reaches a highly nonlinear state, after a given number of e foldings, the local analysis yields a prediction for the propagation distance, z_Γ, at which saturation occurs. As stated in Sec. III, the maximum number of e foldings for a given k is $\Gamma \approx 8(L\omega_{p0}/c)\hat{k}^5\hat{\gamma}_0^2$, which occurs in the neighborhood of $z_\Gamma \approx L(\hat{k}^2 - 1)$. Solving for $\hat{k}$ in the expression for z_Γ and substituting into the expression for Γ results in a relationship between z_Γ and a_0, i.e., $z_0 \propto a_0^{-4/5}$, which can be compared with the simulations. As a criterion for saturation in the simulations, we assume that saturation occurs when the

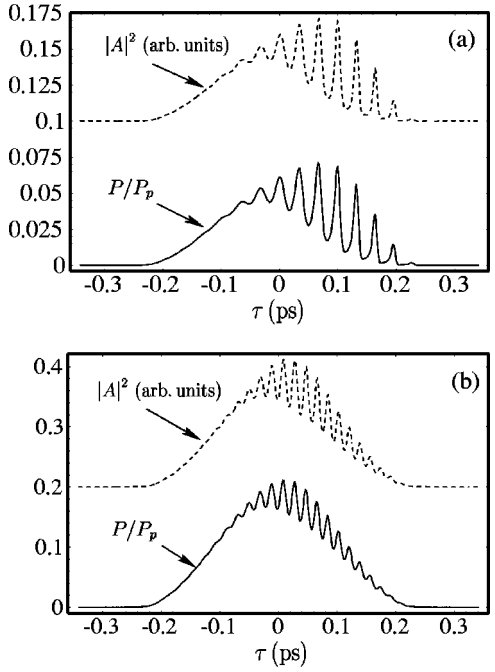

FIG. 8. Longitudinal profiles of scaled power and $|A|^2$ at (a) $z=25\,Z_R$ in an untapered channel and at (b) $z=17\,Z_R$ in a tapered channel corresponding to the spectra displayed in Fig. 6.

modulations grow sufficiently large as to double the laser intensity from its initial peak value. Figure 9 shows the dependence of z_Γ on a_0 obtained from the simulations. The simulations show good agreement with the $a_0^{-4/5}$ scaling predicted by the local analysis over a range in which a_0 and z_Γ vary by more than a factor of 3. Because of the rapid intensity gain near the saturation region, z_Γ does not depend strongly on the arbitrary choice of saturation level, i.e., the plot in Fig. 9 would not change significantly if we had assumed a factor of 3 or 4 intensity gain for the saturation criterion instead of 2.

The next simulation illustrates an interesting case for which no Stokes lines of the laser grow to saturation. The initial laser pulse has $a_0=0.04$, $\lambda=1\ \mu$m, $\tau_L=1$ ps, and $r_0=150\ \mu$m. Figure 10(a) shows the spectrum of this pulse after propagating $2.5\,Z_R$ in an untapered channel with an on-axis density of $n(0)=7\times10^{18}\,\mathrm{cm}^{-3}$. The Stokes sideband is 100 times larger than the anti-Stokes sideband indicating that the Raman instability occurs in the three-wave regime. Figure 10(b) shows the spectrum of the same initial laser pulse after propagating $2.5\,Z_R$ in a tapered channel with $L=7.4\,Z_R$. The initial on-axis density of the tapered channel is the same as that of the untapered channel. Note the appearance of a Stokes structure with three closely spaced peaks. If the evolution of the spectrum in z is examined, the peaks would appear sequentially in the order indicated on the plot with the lowest amplitude peak appearing first. Each peak is seen to grow to a maximum amplitude and decay slightly as the next peak appears.

Figure 11 shows the on-axis laser envelope profile at $z=0$ and $z=2.5\,Z_R$ for propagation in an untapered and a tapered channel. The untapered case shows the appearance of modulations in the laser envelope. Although the modulations

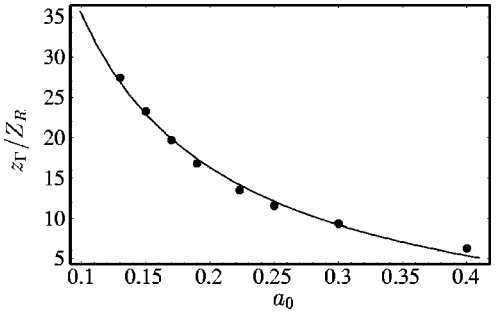

FIG. 9. Dependence of the scaled intensity doubling length z_Γ on a_0. Points represent simulations with parameters $\lambda=1\ \mu$m, $r_0=12.6\ \mu$m, $n(0)=1.24\times10^{19}\,\mathrm{cm}^{-3}$, $\tau_L=0.48$ ps, and $L=20\,Z_R$. The solid curve shows a best fit using the $z_\Gamma\propto a_0^{-4/5}$ dependence predicted by local analysis.

are seen to convect backward in the pulse frame, the convection velocity is slow enough that the modulations can grow to a large amplitude before reaching the back of the pulse. For the tapered channel, since no frequency sidebands grow to a significant amplitude over the propagation length of the simulation, large amplitude modulations of the laser envelope at the plasma frequency are not observed. A careful examination of the laser envelope shows that as each Stokes peak appears in the spectrum of Fig. 10, small amplitude modulations form near the leading edge of the laser envelope. The modulations then rapidly convect out the back of the laser pulse before they can grow to large amplitudes, leaving the laser envelope relatively undistorted. The intensity gain observed in Fig. 11(b) is due to both a longitudinal and transverse compression of the laser pulse.

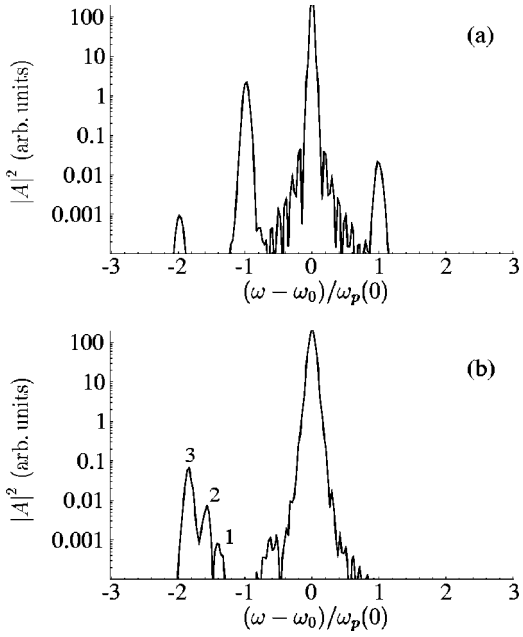

FIG. 10. Frequency spectrum at $z=2.5\,Z_R$ after propagation in (a) an untapered and (b) tapered channel for parameters $a_0=0.04$, $\lambda=1\ \mu$m, $r_0=150\ \mu$m, $n(0)=7\times10^{18}\,\mathrm{cm}^{-3}$, and $\tau_L=1$ ps. For these parameters $P_0/P_p(0)=0.25$. For the tapered channel, $L=7.4\,Z_R$.

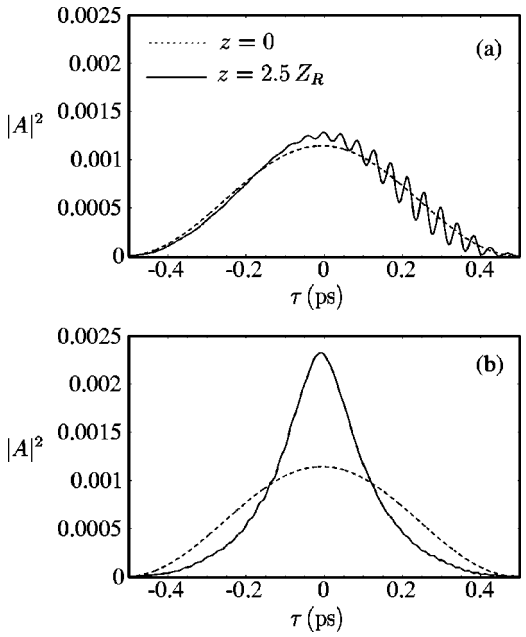

FIG. 11. Scaled amplitudes $|A|^2$ at $z=0$ (dashed curves) and $z=2.5\,Z_R$ (solid curves) for propagation in (a) an untapered and (b) tapered channel for the same simulations as in Fig. 10.

B. Self-modulation instability

The SM instability can occur for a matched, channel-guided pulse even when the laser power $P \ll P_p$ since the channel effectively eliminates diffraction. As the plasma density increases with propagation distance, the critical power for nonlinear self-focusing decreases leading to an increased focusing of the laser pulse. The increased focusing can enhance the SM instability. This is illustrated in the following simulations in which a laser pulse is propagated through a tapered channel in which the on-axis density and channel radius vary as shown in Fig. 5. The initial laser pulse has $a_0=0.5$, $\lambda=1\ \mu$m, $\tau_L=2.4$ ps, and $r_0=40\ \mu$m. The on-axis plasma density at $z=0$ is $n(0)=1.24\times10^{18}\,\mathrm{cm}^{-3}$. The peak laser power P is such that $P=P_p(0)/2$.

Figure 12 shows a plot of $|A|^2$ on-axis and scaled laser power versus τ after propagating a distance of $2.5\,Z_R$. The laser power is normalized to the nonlinear focusing power at $z=2.5\,Z_R$. Although the laser envelope is strongly modulated, no modulations are evident in the power profile. This indicates that the modulations in the laser intensity were caused by a flow of energy transverse to the laser axis, which is characteristic of the SM instability. The ratio of $P/P_p(z)$ has increased from its initial value of $P=0.5\,P_p(0)$ due to the smaller value of P_p at $z=2.5\,Z_R$.

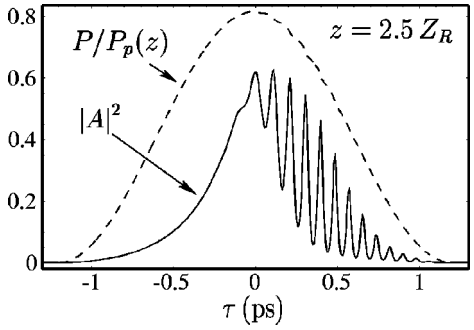

FIG. 12. On-axis profile of $|A|^2$ (solid curve) and normalized laser power (dashed curve) vs τ at $z=2.5\,Z_R$ for an initial laser pulse with $a_0=0.5$, $\lambda=1\ \mu$m, $\tau_L=2.4$ ps, and $r_0=40\ \mu$m. The on-axis plasma density at $z=0$ is $n(0)=1.24\times10^{18}\,\mathrm{cm}^{-3}$. For these parameters, $P_0/P_p(0)=0.5$. The density and channel radius vary as in Fig. 5.

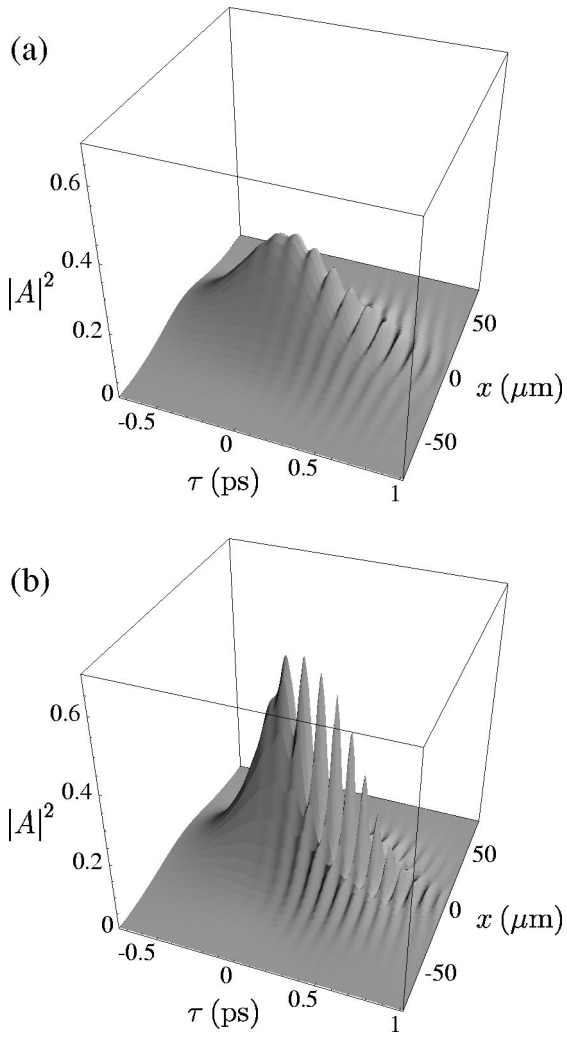

FIG. 13. Surface plots of $|A|^2$ in the x-τ plane at $z=2.5\ Z_R$ after propagation through (a) an untapered channel and (b) a tapered channel in which the radius and density vary as shown in Fig. 5. The initial laser pulse used for both panels is characterized by $a_0=0.5$, $\lambda=1\ \mu$m, $\tau_L=2.4$ ps, and $r_0=40\ \mu$m. The on-axis plasma density at $z=0$ is $n(0)=1.24\times10^{18}\,\mathrm{cm}^{-3}$.

The fact that the modulations are enhanced by relativistic focusing was verified by comparing the simulation of Fig. 12 with two cases in which the nonlinear self-focusing power did not decrease with propagation distance. In the first comparison, the initial conditions were identical except that the channel was not tapered. For this case, self-modulation was observed but with the modulations growing more slowly than when the channel was tapered. Figure 13 shows that, at the same propagation distance, the degree of envelope modu-

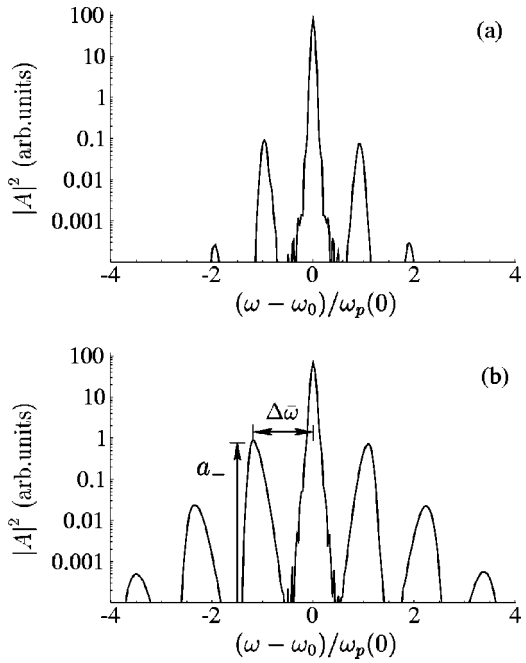

FIG. 14. On-axis frequency spectrum at $z=2.5\,Z_R$ for propagation in (a) an untapered and (b) tapered channel corresponding to the simulation runs shown in Fig. 13.

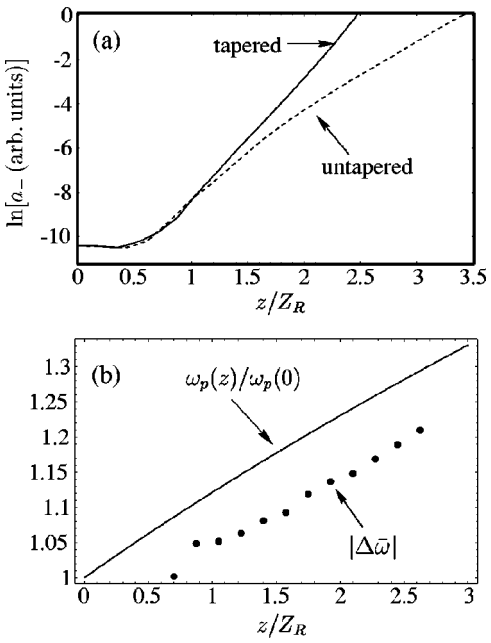

FIG. 15. (a) Amplitude of the Stokes sidebands vs z for the tapered and untapered plasma channels from the simulation of Fig. 14. (b) Normalized frequency shift of the Stokes sideband, $\Delta\bar{\omega}$, vs z for the tapered channel simulation of Fig. 14(b). The solid curve in panel (b) represents the normalized plasma frequency.

lation is much less for propagation in the untapered channel.

The second comparison utilized the same initial laser pulse and tapered channel as the run shown in Fig. 12(b), but artificially held constant the plasma density in the $|a|^3$ term of Eq. (4). As a result, the relativistic focusing effect was not enhanced as the pulse propagated. For this case, the growth of the modulations also progressed more slowly than for the tapered case. Hence, it is reasonable to conclude that while relativistic self-focusing is not a necessary condition for the SM instability, it was the mechanism responsible for enhancing its growth.

Figure 14 shows the on-axis frequency spectrum at $z=2.5\,Z_R$ after propagation in an untapered channel and a tapered channel. Unlike the simulations done in the Raman regime, the Stokes and anti-Stokes sidebands are of equal amplitude and the spectrum is highly symmetric. At any given location z the sidebands for the tapered channel case are larger in amplitude and are broader than for the untapered channel.

The evolution of the Stokes sideband of Fig. 14 is plotted in Fig. 15. Figure 15(a) compares the growth of the Stokes amplitude for a tapered and untapered channel. Unlike the case of the FR instability, the tapered channel does not significantly delay the onset of the instability relative to the untapered channel. This is consistent with the analytical result that detuning is not effective for the SM instability at these parameters (see Fig. 4). Figure 15(b), illustrates the evolution of the Stokes line frequency shift for the tapered channel. Similar to the FR case of Fig. 7, the Stokes frequency shift increases with the local plasma frequency but is smaller than the local plasma frequency at any given z by a constant amount $\approx 0.08\omega_p(0)$.

C. Wake fields in tapered channels

The electron dephasing length is usually defined as the propagation distance required for an electron moving at the speed of light to slip a distance of $\lambda_p/4$ relative to the wakefield. The standard expression for the dephasing length [8,10], $L_D=\gamma_g^2\lambda_p=\lambda_p^3/2\lambda^2$ is derived under the assumption that the phase velocity of the wake, v_w, is equal to the group velocity of the laser pulse, v_g. While this assumption is valid in the short pulse ($c\tau_L<\lambda_p$) regime it may not be accurate in the long pulse regime when the wake is generated primarily by envelope modulations that result from instabilities. In this case, it is more accurate to assume that the phase velocity of the wake will be nearly equal to the phase velocity of the modulations, which need not be equal to the laser pulse group velocity.

For an untapered channel, the approximate phase velocity of the modulations, v_m, can be calculated from the dispersion relation. For example, the fastest growing mode for the SM instability will have $v_m\approx \mathrm{Re}(\omega)/k_p$, where $\omega=\omega_p+\delta\omega$ and $\delta\omega$ is obtained from Eq. (30). The scaled modulation phase velocity, $\beta_m=v_m/c$, in a uniform plasma is then given approximately by

$$\beta_m\approx 1-\frac{1}{2}\left(\frac{a_0\lambda}{16r_0}\right)^{2/3}, \tag{31}$$

where we have chosen $\lambda_\perp=2\pi/k_\perp=4r_0$. Equation (31) indicates that $\beta_m<\beta_g$ when

$$\left(\frac{a_0\lambda}{16r_0}\right)^{2/3}>\frac{\omega_p^2}{\omega_0^2}+\frac{2c^2}{r_0^2}. \tag{32}$$

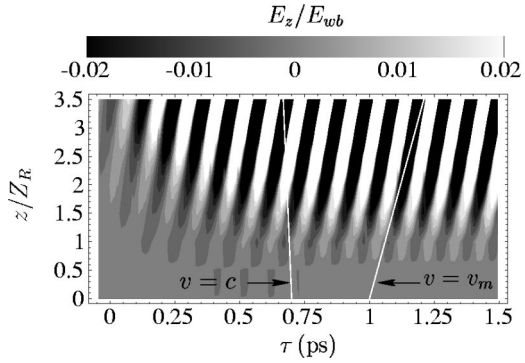

FIG. 16. Level plots of the on-axis longitudinal component of the electric field vs z and τ for propagation in an untapered plasma channel for the same simulation as in Fig. 13(a). Electric field is normalized to $E_{wb}=mc\omega_{p0}/e$.

Hence, a more accurate estimate of the dephasing length for pulses undergoing self-modulation is $L_D'=\gamma_m^2\lambda_p$ where $\gamma_m=(1-\beta_m)^{-1/2}$. As an example, consider a self-modulated laser pulse with $\lambda=1\,\mu$m, $a_0=0.5$, and spot size $r_0=40\,\mu$m in a plasma with density $n_p=1.24\times10^{18}\,\mathrm{cm}^{-3}$ ($\lambda_p=30\,\mu$m). For this example, $\gamma_m=13$ and $\gamma_g=29$, which indicates that $L_D'\approx L_D/5$.

Figure 16 shows a level plot of on-axis E_z/E_{wb} as a function of τ and z resulting from the full-scale simulation. In this type of plot, objects traveling slower (faster) than the laser pulse will trace out a trajectory with a positive (negative) slope. For reference, the thin white curves denote objects traveling at velocities c and v_m, i.e., the theoretical phase velocity of Eq. (31). For this example, it is observed that the phase velocity of the modulations is equal to the phase velocity of the wakefield. The theoretical value of the modulation phase velocity is slightly smaller than the wake phase velocity resulting from the simulation, with a relative error in the relativistic factor, γ of $\approx10\%$. The curve denoting $v=c$ in Fig. 16 indicates that the dephasing distance for a particle traveling near the speed of light is $\approx0.5\,Z_R$. These results are consistent with simulations reported in Ref. [23].

The phase velocity of the wakefield in a longitudinally varying plasma can be expressed in terms of the velocity of modulations, v_m, in a straightforward manner. The wave number of the plasma wave is given by $K_p(z)=\omega_p(z)/v_m(z)$, where the modulation velocity is also taken to vary spatially. Behind the laser pulse, the phase of the plasma wave in the group velocity frame is given by $\psi(z,\tau)=\omega_p[(v_m^{-1}-v_g^{-1})z-(\tau-\tau_0)]$, where τ_0 is an arbitrary constant which fixes the phase. In the laboratory frame, the frequency and wave number associated with the plasma wave are $\Omega=-\partial\psi/\partial\tau$ and $K=[(\partial/\partial z)-v_g^{-1}(\partial/\partial\tau)]\psi$, respectively. Hence, the phase velocity of the plasma wave is

$$v_w(z,\tau)\equiv\frac{\Omega}{K}=v_m(z)\left\{1-\frac{\omega_p'}{\omega_p}v_m\left[\tau-\tau_0-\left(\frac{1}{v_m}-\frac{1}{v_g}\right)z\right]+z\left(\frac{v_m v_g'}{v_g^2}-\frac{v_m'}{v_m}\right)\right\}^{-1},\qquad(33)$$

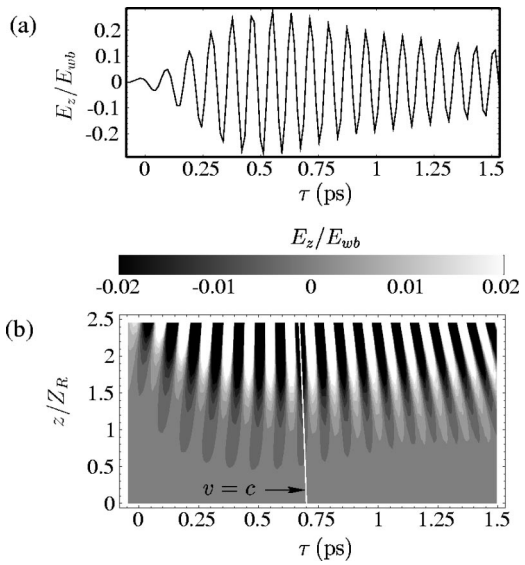

FIG. 17. (a) Normalized on-axis longitudinal component of the electric field at $z=2.5\,Z_R$ associated with the laser pulse of Fig. 13(b). Electric field is normalized to $E_{wb}=mc\omega_{p0}/e$. Panel (b) shows a level plot of the on-axis longitudinal electric field vs z and τ for propagation in a tapered channel for the same simulation as in Fig. 13(b).

where a prime denotes a derivative in z. For the parameters considered here, terms proportional to v_m' and v_g' do not contribute significantly to the phase velocity. In the absence of a density gradient we recover $v_w=v_m$. Also, in the short-pulse regime we can set $v_m=v_g$ and recover, essentially, Eq. (30) of Ref. [8], which gives the wakefield phase velocity for a tapered channel in the short-pulse limit.

Figure 17(a) shows the profile of the longitudinal electric field associated with the laser pulse shown in Fig. 13(b). The wakefield amplitude increases in τ to a peak amplitude of $E_z=0.27E_{wb}$, where $E_{wb}=mc\omega_{p0}/e\approx110$ GV/m, and then slowly damps for $\tau>0.5$ ps. The damping is an effect associated with the radial variation of the plasma density and has been observed in earlier works [44]. In the tapered channel, the wakefield in the neighborhood of $\tau=0.7$ ps has a phase velocity close to c as shown in Fig. 17(b). It has been shown previously that particles injected into this luminal region of the wake can be accelerated to energies beyond the dephasing limit [8]. This appears to be a way to mitigate the phase slippage problem seen in other simulations of the channel-guided self-modulated LWFA [23].

The fractional energy spread acquired by a distribution of electrons injected in the vicinity of the luminous point of the wake is given by

$$\Delta_W(z)=\frac{W(0,z)-W(\delta\tau,z)}{W(0,z)}\approx\frac{\omega_{p0}^2\delta\tau^2}{2}\left(1+\frac{z}{L_0}\right),\qquad(34)$$

where $\delta\tau=\tau-\tau_c$, τ_c denotes the axial coordinate of the luminous point, $W(0,z)$ denotes the energy gained by an electron injected at the luminous point, $W(\delta\tau,z)$ denotes the energy gained after a distance z by an electron initially displaced by $\delta\tau$ from the luminous point, ω_{p0} is the on-axis

plasma density at $z=0$, and $L_0=\omega_p/\omega_p'|_{z=0}$ is the density scale length at $z=0$. In deriving Eq. (34) it has been assumed that $z \ll L_0$, $\omega_{p0}\delta\tau \ll 1$, the wake field amplitude is constant, and that the electrons are injected with an initial energy $W(\delta\tau,0) \ll W(\delta\tau,z)$. It is also assumed that the luminous point occurs where the accelerating field is maximum and that its phase is constant (see Fig. 17). Using Eq. (34), we find that for the parameters of Fig. 17, i.e., $\lambda_{p0}=30\,\mu$m and $L_0 \sim 2$ cm, an electron bunch of duration ~ 5 fsec will acquire a fractional energy spread of $\sim 7\%$ after propagating a distance of ~ 1 cm.

VI. CONCLUSIONS

We have investigated the propagation of intense laser pulses with pulse durations greater than the plasma period in tapered plasma channels. Reduced partial differential equations that separately describe the FR and SM instabilities in a longitudinally varying plasma were derived and a heuristic analysis of the detuning of these instabilities was presented. An illustrative case of a linearly increasing plasma density was considered to identify the relevant scalings that characterize the detuning process. The analysis shows that the FR instability can be easily detuned since a given wave number is unstable only within a limited spatial region (see Fig. 2). For the SM instability, the detuning process is not as effective since the unstable region is much broader in extent (see Fig. 4).

Full-scale numerical simulations of propagation in tapered plasma channels were preformed and parameters that favorably excite either the FR or SM instability were found. The forward Raman simulations exhibited modulations of the laser intensity caused by the longitudinal bunching of energy (see Fig. 8). Detuning of the FR instability in a tapered channel was observed. For example, Fig. 7 shows that the growth of the Stokes line is delayed in a tapered channel relative to an untapered channel and that the frequency of the Stokes line varies with propagation distance. Simulations showed that laser pulses undergoing a self-modulation instability in a plasma channel are characterized by modulations arising from the transverse flow of energy. As seen in Fig. 14, these self-modulated pulses exhibit highly symmetric spectra. For a tapered channel in which the plasma density increases in the direction of propagation, it was shown that the growth of the SM instability is enhanced by relativistic focusing. It is also evident from Fig. 15 that, unlike the FR instability, the tapered channel did not delay the growth of the SM instability.

The phase velocity of the wake field generated by the SM instability was analyzed. For propagation in a uniform plasma, the phase velocity of the wake is smaller than the group velocity of the laser pulse when the condition given by Eq. (32) is satisfied. Equation (31), which gives the phase velocity of the wake, was found to be in good agreement with the simulation presented in Sec. V. Results indicate that the slower phase velocity of the wake should be taken into account for an accurate calculation of the dephasing length.

Simulations show that in a tapered channel, the wake field phase velocity can be equal to c at some location behind the pulse. The wake field amplitude, however, initially increases and then decreases towards the back of the pulse. For the example shown in Fig. 17, the phase velocity of the wake becomes equal to c in the region where the wakefield amplitude is maximum. The larger wake field amplitude occurring within the luminal part of the wake provides the ideal condition for accelerating high-energy electrons. An optical injection scheme capable of producing short ($\sim$fsec) electron bunches, such as the colliding pulse injector [46], may be necessary to limit the energy spread of the accelerated particles. These results suggest that a self-modulated LWFA utilizing a tapered channel may be a viable near-term experiment.

ACKNOWLEDGMENTS

This work was supported by the DOE and ONR.

[1] A. Goltsov *et al.*, IEEE J. Sel. Top. Quantum Electron. **5**, 1453 (1999).
[2] M. Tabak, J. Hammer, M. Glinsky, W. Kruer, S. Wilks, J. Woodworth, E. Campbell, M. Perry, and R. Mason, Phys. Plasmas **1**, 1626 (1994).
[3] S. Wilks and W. Kruer, IEEE J. Quantum Electron. **33**, 1954 (1997).
[4] E. Esarey, P. Sprangle, J. Krall, and A. Ting, IEEE J. Plasma Sci. **PS-24**, 252 (1996).
[5] T. Katsouleas, Phys. Rev. A **33**, 2056 (1986).
[6] S. Bulanov, N. Naumova, F. Pegoraro, and J. Sakai, Phys. Rev. E **58**, R5257 (1998).
[7] L. Gorbunov, V. Kirsanov, S. Mtingva, and R. Ramazashvill, Kratk. Soobshch. Fiz. **10**, 27 (1989).
[8] P. Sprangle, B. Hafizi, J. Peñano, R. Hubbard, A. Ting, C. Moore, D. Gordon, A. Zigler, D. Kaganovich, and T. Antonsen, Phys. Rev. E **63**, 056405 (2001).
[9] R. Hubbard, P. Sprangle, and B. Hafizi, IEEE Trans. Plasma Sci. **28**, 1159 (2000).
[10] R. Hubbard, D. Kaganovich, B. Hafizi, C. Moore, P. Sprangle, A. Ting, and A. Zigler, Phys. Rev. E **63**, 036502 (2001).
[11] D. Kaganovich, P. Sasorov, C. Cohen, and A. Zigler, Appl. Phys. Lett. **75**, 772 (1999).
[12] A. Borisov *et al.*, Phys. Rev. Lett. **68**, 2309 (1992).
[13] A. Sullivan, H. Hamster, S. Gordon, R. Falcone, and H. Nathel, Opt. Lett. **19**, 1544 (1994).
[14] P. Monot, T. Auguste, P. Gibbon, F. Jakober, G. Mainfray, A. Dulieu, M. Louis-Jacquet, G. Malka, and J. Miquel, Phys. Rev. Lett. **74**, 2953 (1995).
[15] C. Coverdale, C. Darrow, C. Decker, W. Mori, K. Tzeng, K. Marsh, C. Clayton, and C. Joshi, Phys. Rev. Lett. **74**, 4659 (1995).
[16] A. Modena *et al.*, Nature (London) **337**, 606 (1995).
[17] K. Nakajima *et al.*, Phys. Rev. Lett. **74**, 4428 (1995).

[18] D. Umstadter, S. Chen, A. Maksimchuck, G. Mourou, and R. Wagner, Science **273**, 472 (1996).
[19] H. Milchberg, T. Clark, C.G. Durfee III, T. Antonsen, and P. Mora, Phys. Plasmas **3**, 2149 (1996).
[20] A. Zigler, Y. Erhlich, C. Cohen, J. Krall, and P. Sprangle, J. Opt. Soc. Am. B **13**, 68 (1996).
[21] Y. Erhlich, C. Cohen, A. Zigler, J. Krall, P. Sprangle, and E. Esarey, Phys. Rev. Lett. **77**, 4186 (1996).
[22] A. Ting, C. Moore, K. Krushelnick, C. Manka, E. Esarey, P. Sprangle, R. Hubbard, H. Burris, R. Fischer, and M. Baine, Phys. Plasmas **4**, 1889 (1997).
[23] P. Sprangle, J. Peñano, B. Hafizi, R. Hubbard, A. Ting, D. Gordon, A. Zigler, and T. Antonsen, Phys. Plasmas **9**, 2364 (2002).
[24] J. Drake, P. Kaw, Y. Lee, G. Schmidt, C. Liu, and M. Rosenbluth, Phys. Fluids **17**, 778 (1974).
[25] K. Estabrook and W. Kruer, Phys. Fluids **26**, 1892 (1983).
[26] C. McKinstrie and R. Bingham, Phys. Fluids B **4**, 2626 (1992).
[27] T. Antonsen and P. Mora, Phys. Fluids B **5**, 1440 (1993).
[28] W. Mori, C. Decker, D. Hinkel, and T. Katsouleas, Phys. Rev. Lett. **72**, 1482 (1994).
[29] C. Decker, W. Mori, and T. Katsouleas, Phys. Rev. E **50**, R3338 (1994).
[30] D. Gordon, B. Hafizi, P. Sprangle, R. Hubbard, J. Peñano, and W. Mori, Phys. Rev. E **64**, 046404 (2001).
[31] E. Esarey, J. Krall, and P. Sprangle, Phys. Rev. Lett. **72**, 2887 (1994).
[32] J. Krall, A. Ting, E. Esarey, and P. Sprangle, Phys. Rev. E **48**, 2157 (1993).
[33] W. Mori, IEEE J. Quantum Electron. **33**, 1942 (1997).
[34] G. Shvets and X. Li, Phys. Plasmas **8**, 8 (2001).
[35] M. Rosenbluth, Phys. Rev. Lett. **29**, 565 (1972).
[36] T. Tajima and J. Dawson, Phys. Rev. Lett. **43**, 267 (1979).
[37] P. Sprangle, E. Esarey, A. Ting, and G. Joyce, Appl. Phys. Lett. **53**, 2146 (1988).
[38] N. Andreev, L. Gorbunov, V. Kirsanov, K. Nakajima, and A. Ogata, Phys. Plasmas **4**, 1145 (1997).
[39] N. Andreev, L. Gorbunov, and A. Frolov, Plasma Phys. Rep. **24**, 825 (1998).
[40] E. Esarey, C. Schroeder, B. Shadwick, J. Wurtele, and W. Leemans, Phys. Rev. Lett. **84**, 3081 (2000).
[41] P. Sprangle, B. Hafizi, J. Peñano, R. Hubbard, A. Ting, A. Zigler, and T. Antonsen, Phys. Rev. Lett. **85**, 5110 (2000).
[42] C. Max, J. Arons, and A. Langdon, Phys. Rev. Lett. **33**, 209 (1974).
[43] P. Sprangle, C. Tang, and E. Esarey, IEEE Trans. Plasma Sci. **PS-15**, 145 (1987).
[44] E. Esarey, P. Sprangle, J. Krall, and A. Ting, IEEE J. Quantum Electron. **33**, 1879 (1997).
[45] P. Sprangle, E. Esarey, and A. Ting, Phys. Rev. A **41**, 4463 (1990).
[46] E. Esarey, R. Hubbard, W. Leemans, A. Ting, and P. Sprangle, Phys. Rev. Lett. **79**, 2682 (1997).